Dissociative electron attachment in nanoscale ice films: Temperature and morphology effects

W. C. Simpson, M. T. Sieger, and T. M. Orlando[a)]
W. R. Wiley Environmental Molecular Sciences Laboratory, Pacific Northwest National Laboratory, P.O. Box 999, M/S K8-88, Richland, Washington 99352

L. Parenteau, K. Nagesha, and L. Sanche[a)]
Canadian Medical Research Group in Radiation Sciences, Faculty of Medicine, University of Sherbrooke, Sherbrooke, Québec, Canada, J1H 5N4

(Received 11 July 1997; accepted 20 August 1997)

The electron-stimulated desorption (ESD) of D^- ions from condensed D_2O films is investigated. Three low-energy peaks are observed which are identified as arising from excitation of $^2B_1$, $^2A_1$, and $^2B_2$ dissociative electron attachment (DEA) resonances. A fourth, higher energy feature is also seen in the D^- yield which is likely due to the formation of a transient anion state that dissociates and/or decays into a dissociative excited state. The energies and ion yields of the resonances vary with the temperature and morphology of the D_2O film. Below 60 K, the work function of the ice films changes with temperature and the DEA resonances shift in energy. The D^- ESD yield generally increases with temperature, but it deviates from this trend at temperatures corresponding to structural phase transitions in ice. The ($^2B_1$) D^- temperature dependence is remarkably similar to that observed for the ESD of low-energy D^+ ions from D_2O ice, even though the two originate from different electronic excitations. These results are attributed to thermally induced changes in the hydrogen bonding network, which changes the lifetimes of the predissociative states that lead to ESD and which also allows for the reorientation of surface molecules. © *1997 American Institute of Physics.* [S0021-9606(97)02344-1]

I. INTRODUCTION

Resonance structure is often observed in the cross sections for low-energy electron scattering from isolated molecules due to the formation of transient negative ion states, which decay either via electron autodetachment or dissociative electron attachment (DEA). DEA typically involves multielectron resonances consisting of an excess electron bound temporarily to an electronically excited molecule. These core-excited transient anion states are generally two-electron, one-hole configurations which are classified as either Feshbach or shape resonances. Since the lifetimes of Feshbach resonances are sufficiently long ($\sim 10^{-12}$ -10^{-14} s) for significant nuclear motion to occur, dissociation into stable anion and neutral fragments will result provided one of the fragments has a positive electron affinity and that the excited anionic state is symmetry allowed and dissociative in the Franck–Condon region.

Resonance structure is also observed in the electron scattering and electron stimulated desorption (ESD) cross sections of condensed molecules.[1–5] Since these resonances are highly localized, they can be conceptualized using a single-site scattering picture. However, additional factors must be considered due to the influence of the surrounding medium. These include: (1) changes in the symmetry of the scattering event, (2) the fixed orientation of the molecule with respect to the surface, (3) the polarization response of the medium, (4) short-range interactions between the molecules, (5) image interactions with the substrate, (6) the occurrence of new decay channels, (7) inelastic scattering of the incident electron, and (8) in the case of DEA, postdissociation interactions between the ion fragment and the surrounding medium.[1–12] To date, there are no predictive models that specify which of these factors have the greatest influence in a particular system. Hence, it is of general interest to investigate how condensation affects electron-molecule scattering in various systems.

Water has obvious biological and chemical significance, and it is also an excellent substance for investigating the effects of condensation on DEA. The vapor pressure of water below $\sim$175 K is less than 10^{-5} Torr,[13] which is sufficiently low to enable the investigation of water films under ultrahigh vacuum (UHV) conditions over a wide temperature range. Water films are also highly polarizable and exhibit a number of morphologies which depend on the growth conditions and film temperature. In addition, hydrogen bonding interactions between neighboring water molecules can, in principle, affect DEA resonance energies and ESD ion yields.

The DEA resonances in water vapor are well characterized.[14–27] Three distinct $(H_2O^-)^*$ states have been observed for incident electron energies (E_i) below 15 eV. Each of these Feshbach resonances, which are peaked at 6.5, 8.6, and 11.8 eV, generate H^-, O^-, and OH^-, although the cross sections for O^- and OH^- production are quite low. The measured angular distributions of H^- are consistent with resonances of symmetry $^2B_1$ (6.5 eV), $^2A_1$ (8.6 eV), and $^2B_2$ (11.8 eV).[14] The energies of these DEA resonances are essentially unchanged upon isotopic substitution. However, the cross section for D^- production from D_2O is reduced by a

[a)]Authors to whom correspondence should be addressed.

factor of ~0.6 from that of H^- from H_2O, and the widths of the resonances are reduced by ~0.3 eV.[15]

The ESD of H^-/D^- via DEA has been observed in thin films of condensed H_2O and D_2O, and in submonolayer water films adsorbed on noble gas multilayers.[9,12,28] The H^-/D^- ESD yield has a threshold at ~5.5 eV and it peaks at ~7.4 eV, with a shoulder at ~9 eV.[9] This structure in the anion yield was attributed to excitation of the $^2B_1$ and $^2A_1$ DEA resonances, respectively, which are ~1 eV higher in energy and broader than in the gas phase. The energy shift was attributed to perturbations of the electronic structure of water upon condensation.[9] When D_2O is substituted for H_2O, the main ($^2B_1$) DEA resonance narrows in the same manner as is seen in the gas phase, indicating that inelastically scattered electrons do not contribute significantly to the width of the resonance.[9] Instead, the increased width of the resonance was ascribed to condensation-induced changes in the potential energy surfaces involved in the dissociation process. Energy- and angle-resolved D^- ESD measurements from D_2O multilayers reveal additional differences between anion production in gas- and condensed-phase water. At low E_i, the most probable kinetic energy of the desorbing anions increases linearly with energy, having a slope close to that seen in the gas phase (0.4 eV/eV).[12] However, the ion kinetic energy distributions are shifted down by ~0.5 eV and are noticeably broader. In addition, the measured angular distributions of the desorbing ions do not reflect the symmetry of the transient excited states, as they do in the gas phase. Instead, they peak in the surface normal direction.[12] Finally, electron energy-loss measurements of H_2O multilayers indicate that condensation opens up an additional decay channel for the $^2B_1$ Feshbach resonance which can couple, via long-range dipole interactions, to intermolecular vibrational modes of the surrounding film.[8]

In this article we demonstrate that the energies and ion yields of the three low-energy DEA resonances depend on the temperature and morphology of the film. We also report a fourth, higher energy feature in the D^- yield which may be associated with a DEA resonance and/or the creation of ion pairs. We discuss how the temperature and morphology dependence of the ion yields results from changes in the hydrogen bonding network and from the reorientation of surface molecules. The experimental procedure and sample preparation techniques are described in Sec. II. A discussion of the energy, temperature, and morphology dependence of the D^- ESD yield is presented in Sec. III. Finally, a summary of our observations and conclusions is presented in Sec. IV.

II. EXPERIMENTAL PROCEDURE

A. Ultrahigh vacuum systems and techniques

The experiments were carried out at Pacific Northwest National Laboratory (PNNL) and at the University of Sherbrooke. The PNNL apparatus consists of an UHV chamber (base pressure $\sim 2\times10^{-10}$ Torr) equipped with a pulsed low-energy electron gun, an effusive gas doser, a quadrupole mass spectrometer (QMS), a time-of-flight (TOF) detector, and a Pt (111) crystal mounted on a liquid-nitrogen-cooled manipulator. The Pt crystal was cleaned by repeatedly heating it to ~1200 K in O_2 (5×10^{-8} Torr) and then in UHV. The temperature was measured with a K-type thermocouple, spot welded to the side of the crystal. For temperature programmed desorption (TPD) and temperature-dependent ESD measurements, the ice films were heated radiantly using a tungsten filament mounted behind the Pt crystal.

The films were grown via vapor deposition of ultrapure D_2O. A calibration of the film thickness and temperature was made by comparing D_2O TPD spectra to computer models and to published data.[29–33] Based on this calibration, we estimate an uncertainty of ± 5 K in the temperature and ~20% in the coverage. Coverages are reported here in terms of ice bilayers ($\sim 10^{15}$ molecules/cm^2).[34]

In the PNNL apparatus, a monochromatic electron beam, having an energy spread of 0.3 eV full width at half-maximum (FWHM), was focused onto D_2O ice films grown on the Pt (111) crystal. The desorbing D^- ions were collected using a 50 V pulse to accelerate them into the TOF spectrometer for detection via gated integration. Accelerating the low-energy ions into the detector guarantees that ions emitted at all angles from the surface are collected and also eliminates any energy bias the detector may have. The incident electron beam was pulsed at 100 Hz, with a pulse duration of 1 μs and an instantaneous current density of $\sim 7\times10^{-7}$ A in a spot size of ~10 mm^2 (7×10^{-10} A/cm^2 time-averaged current density). Under these conditions the D^- signal is linear in the incident electron flux and exhibits well-resolved structure as a function of E_i. Increasing the time-averaged current density by more than a factor of 2 from this value, however, leads to a noticeable loss of resolution in the observed electron energy dependence.[35] The D^- energy and temperature dependence data collected at PNNL are the sum of five to ten separate scans, each typically collected from a freshly grown film. Since the electron flux to the sample changes slightly with E_i, the data are normalized to the incident electron current. Hence, the reported D^- yield represents the number of ions generated per incident electron, which is on the order of 10^{-5}. This normalization does not introduce any additional structure to the data.

The Sherbrooke ESD apparatus and experimental techniques have been described in detail elsewhere.[7,9,10] In brief, the system consists of an UHV chamber (base pressure $\sim 2\times10^{-10}$ Torr) containing a cryo-cooled polycrystalline Pt foil, a low-energy electron monochromator (80 meV FWHM), and a QMS. The Pt foil was cleaned by resistive heating. Doubly distilled D_2O was vapor-deposited on the foil. Film thickness was estimated using a volumetric dosing technique,[36] and has an estimated accuracy of ~50%. D^- ions were generated by the impact of a monochromatic electron beam (5×10^{-9} A in a 12 mm^2 spot, or 4×10^{-8} A/cm^2) and detected using the QMS. Heating was achieved by turning off the cooling system and allowing the film to warm slowly from the base temperature of 23 K.

Low-energy electron transmission (LEET) measurements were also carried out at Sherbrooke using a similar sample preparation method. Details of the LEET apparatus

and technique can be found in Refs. 37 and 38. For the LEET measurements, a magnetically collimated monochromatic electron beam (FWHM~40 meV) impinges on an ice film condensed onto a polycrystalline Pt foil. A LEET spectrum is obtained by collecting the electron current transmitted through the film to ground as a function of the potential applied between the electron source and the Pt substrate. The transmitted electron current rises sharply at the zero energy reference (ZER) of the vacuum level, producing a structure called the injection curve. The half-height of this curve defines the ZER, within the beam resolution, and variations in the work function of the sample cause the ZER to shift in an equivalent manner.

B. Ice film preparation

Four known ice polymorphs, two amorphous and two crystalline, are stable under UHV conditions in the temperature range considered here (23–190 K). Ice films grown by vapor deposition at substrate temperatures below ~110 K are amorphous and have a large surface-to-volume ratio arising from a high density of micropores.[32] These pores collapse if the film is warmed to ~120 K, resulting in a higher density form of amorphous ice.[39–43] Nonporous amorphous ice can also be grown directly by depositing water vapor at temperatures between ~110–140 K. Annealing an amorphous ice film above the amorphous-to-crystalline phase transition temperature (~155 K for the conditions used in this study) leads to crystallization of the film.[33,41,44] Crystalline films can also be grown directly by depositing water vapor at temperatures above ~150 K but below the onset for appreciable D_2O desorption, which is ~160 K. Since we cannot discern from our measurements whether our growth conditions produce hexagonal $I_h(0001)$ or cubic $I_c(001)$ ice, which differ only in their bilayer stacking sequence, we simply refer to these films as crystalline. Note that, depending on the type of water (H_2O or D_2O) and the rate of heating, the temperatures given above may vary by as much as 10 K.[33,42,44]

III. RESULTS AND DISCUSSION

A. Energy dependence of the D^- yield

The energy dependence of the D^- ESD yield from D_2O ice, shown in Fig. 1, exhibits several resonances. There are two intervals, 5–14 eV and 18–32 eV, in which the D^- signal rises significantly above the baseline. While the higher energy feature appears to be a single broad peak, the region below 15 eV is composed of three separate features. As shown in the inset, the signal peaks at ~7 eV, with a pronounced shoulder at ~9 eV and a slightly less intense feature at ~11 eV. A sum of three Gaussian peaks and a linearly increasing background fits this data reasonably well. The baseline gradually increases with E_i in the TOF data in Fig. 1, which is not observed when using a QMS for detection. Below ~16 eV, the roughly linear increase in the baseline with E_i most likely results from a rise in the number

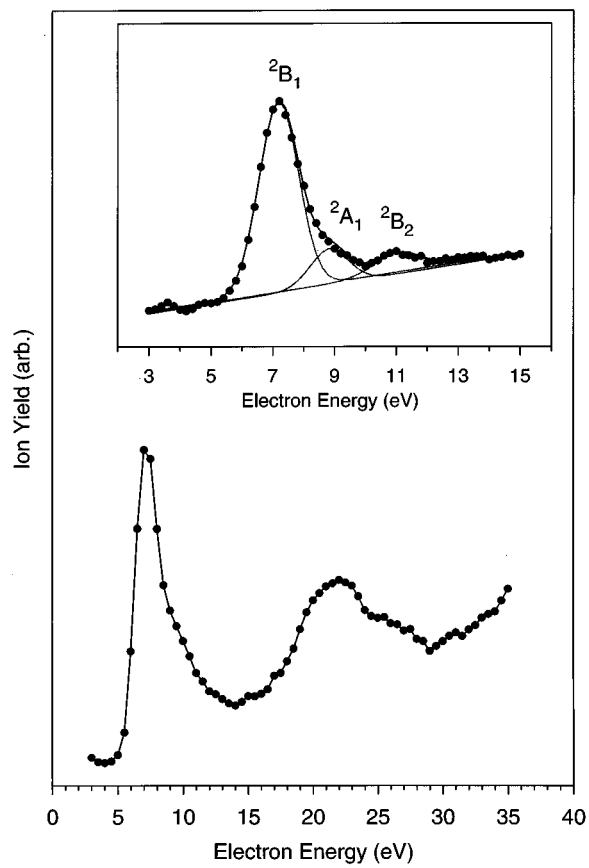

FIG. 1. D^- signal vs incident electron energy, collected at 120 K from a five-bilayer film of amorphous ice, which was grown at 90 K. The inset contains a more detailed scan in the energy range 3–15 eV, along with a fit to the data (see text).

of scattered electrons that pass through the TOF tube. Above ~16 eV, dipolar dissociation also contributes to the baseline.

A schematic representation of the electronic structure of water vapor and ice is given in Fig. 2. The ground state of an isolated water molecule is $(1a_1)^2(2a_1)^2(1b_2)^2(3a_1)^2(1b_1)^2$, where the $1a_1$ orbital is essentially the O($1s$) core level, the $2a_1$ and $1b_2$ orbitals are primarily involved in O–H bonding, and the $3a_1$ and $1b_1$ are nonbonding lone-pair orbitals.[45,46] The two lowest-lying unoccupied orbitals are the $4a_1$ and $2b_2$.[45] The strongly antibonding $4a_1$ orbital mixes with the $3s$ Rydberg state,[47] and hence is denoted as $3s{:}4a_1$.

In many regards, the electronic structure of ice varies little from that of water vapor. The $2b_2$ orbital is apparently replaced by the conduction band and the other valence levels are broadened and shifted slightly in energy.[31,46,48–54] Calculations indicate that the a_1 bands exhibit the most dispersion, whereas the $1b_1$ and $1b_2$ levels are essentially dispersionless.[55,56] The unoccupied $4a_1$ level is in the band gap and is expected to be localized (excitonic) in nature.[54] The conduction band is rather narrow, with the band minimum only ~1 eV below the vacuum level,[49] and the Fermi level is estimated to be roughly 5 eV above the $1b_1$ band maximum.[51]

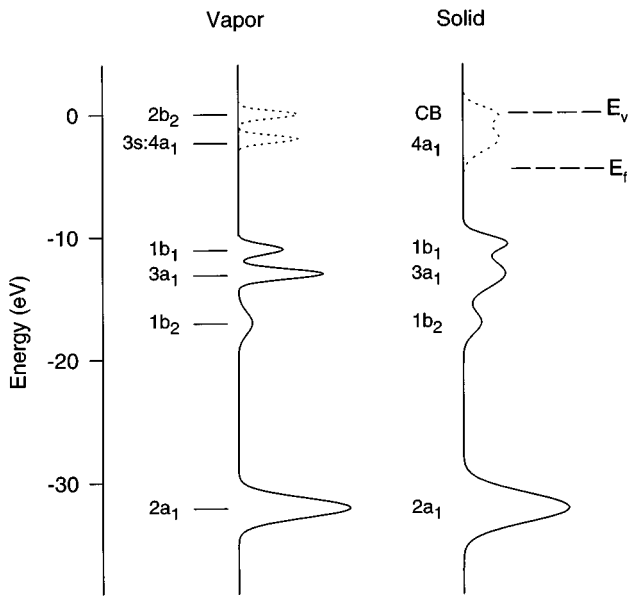

FIG. 2. Schematic representation of the electronic structure of water vapor and ice. The vacuum level and Fermi level are indicated in the figure as E_v and E_f, respectively.

We attribute the low-energy structure in the D^- ESD yield to three DEA resonances in water. The $^2B_1$, $^2A_1$ and $^2B_2$ resonances, which correspond to states having two $3s{:}4a_1$ electrons and a hole in the $1b_1$, $3a_1$, or $1b_2$ orbital, respectively, have been observed in water vapor, where the ratio of their cross sections for H^- production is about 600:120:1, respectively.[14,20] The antibonding nature of the $3s{:}4a_1$ orbital makes these excited states highly dissociative. Observations of simultaneous charge and energy transfer from negatively charged excitons in rare-gas films to physisorbed H_2O molecules[28,57] indicate that, while much of the Rydberg character of this level may be lost upon condensation, at least some is retained. The $4a_1$ level also retains much of its dissociative nature since both the $^2B_1$ and $^2A_1$ resonances have been observed previously to generate measurable D^- ESD yields from condensed water films.[9,12] The energies and intensities of the two lowest-energy peaks in Fig. 1 are consistent with these earlier ESD measurements,[9,12] and are therefore assigned as the $^2B_1$ and $^2A_1$ DEA resonances, respectively. The third feature, at $\sim$11 eV, is only resolvable at very low current densities[58] and has not been observed previously in ESD studies. Maintaining the correspondence between gas-phase and condensed-phase results, we assign this feature to the $^2B_2$ Feshbach resonance.

We consider two possible explanations for the broad feature between $\sim$18 and 32 eV. Since studies of negative ion resonances are often limited to electron energies below 20 eV, there is no report of such a high-energy feature in the H^-/D^- yield from water vapor with which to compare. Similar structure has been observed at $\sim$22–38 eV in the O^- DEA yield from H_2O vapor and is attributed to the onset of ion pair formation.[21,22] The energies required to generate D^- from D_2O vapor via ion pair formation are estimated to be $\sim$22 and 36 eV but may be somewhat lower for condensed water because of dielectric screening. *A priori*, ion pair formation could lead to the structure in the D^- signal at $\sim$18–32 eV. However, unless the cross sections for ion pair formation include the effect of resonances, they are expected to increase monotonically with energy from threshold. It is therefore highly plausible that negative ion resonances associated with a hole in the $2a_1$ orbital are responsible for the 22 eV maximum seen in Fig. 1. Kimmel and Orlando recently observed nearly identical structure in the D_2 yield resulting from the electron bombardment of D_2O ice.[59] The yield of D_2 in the ($J=0$, $v=0$, 2) states increases noticeably between 18 and 32 eV, but no corresponding change is seen for the ($J=0$, $v=1$) state. This propensity to occupy only certain vibrational states seems inconsistent with ion pair formation. Instead, the existence of a negative ion resonance associated with excitation of the $2a_1$ orbital was proposed to explain these results, with the width of the peak resulting from satellites associated with decay of the deep $2a_1$ valence level.[59] The production of D^- through similar excitations can also explain the higher energy structure observed in the ESD yield.

B. Temperature and morphology dependence of the D^- yield

An ESD excitation must remain localized for a sufficiently long time that significant nuclear motion can occur prior to decay. Therefore, the lifetime of the dissociative transient anion state determines, in large part, the D^- ESD yield from D_2O ice. Since DEA involves localization of the attached electron, the lifetimes of DEA resonances (and hence their ESD cross sections) are expected to be sensitive to the *local* potential which, in turn, varies with the film's morphology and temperature. This effect should be most evident in water films, where short-range interactions between neighboring molecules perturb their local electronic structure. To investigate this effect we measured the temperature dependence of the negative-ion ESD yield from crystalline and amorphous ice films.

The temperature dependence of the D^- signal from 20 bilayers of porous amorphous ice, grown at 27 K, is shown in Fig. 3. Both the resonance energies and the ion yields change with temperature. An analysis of the D^- onset energy and the energy and intensity of the low-energy resonance peak indicates that there is a break in this behavior at around 60 K. The peak intensity increases fivefold between 27 and 60 K, remains roughly constant between 60 and 100 K, then more than doubles in going from 100 to 140 K. From 27 to 60 K, the onset and peak energies shift down $\sim$1.6 eV, whereas above 60 K the onset and peak energies are essentially unchanged.

Changes in the work function of the ice film account for less than half of the observed energy shifts. Figure 4 shows the results of LEET measurements carried out on a ten-bilayer H_2O film grown at 23 K. The temperatures at which the data were collected are indicated in the figure. The LEET spectra clearly shift to lower energy with temperature in a

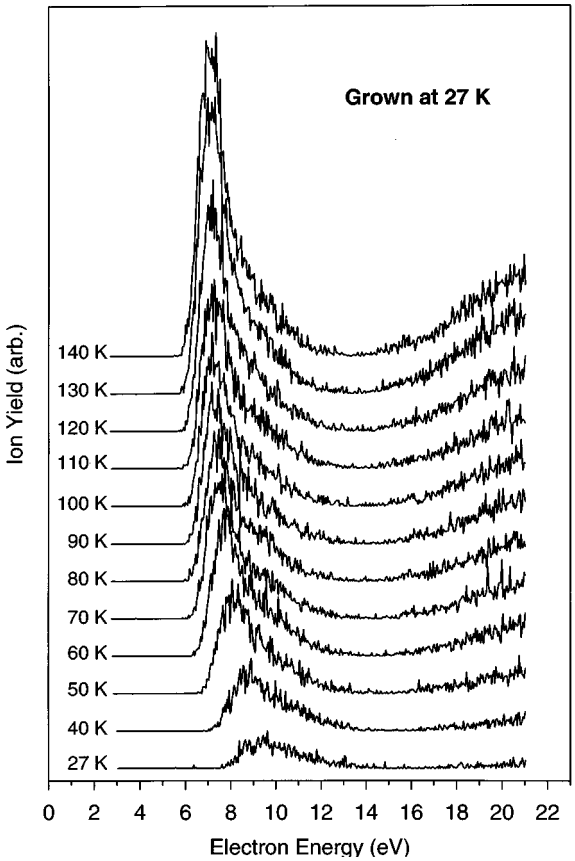

FIG. 3. D^- signal vs incident electron energy, collected at various temperatures from 20-bilayer porous amorphous ice films (grown at 27 K). Individual scans are offset vertically for display and are labeled with the temperature at which they were collected. The films were heated by simply turning off the cryocooler and allowing the films to warm up.

manner similar to the DEA resonances. For a more direct comparison, a plot of the ZER versus temperature is given in Fig. 5, along with the peak and onset energies for D^- ESD from Fig. 3. Although the energy shifts do not have an exact

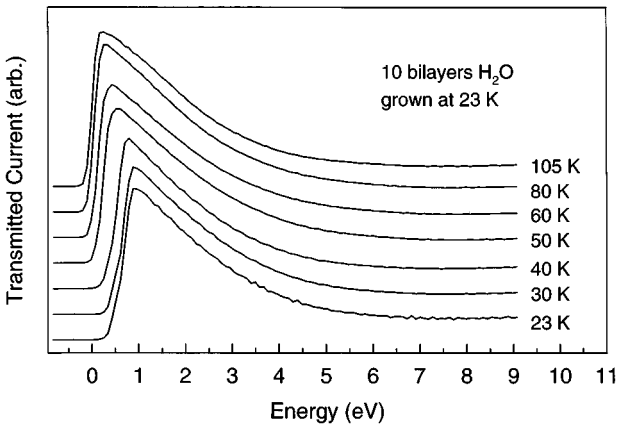

FIG. 4. Low-energy electron transmission spectra collected from a 10-bilayer H_2O ice film grown at 23 K. Individual scans are labeled with their collection temperature and are offset vertically for display. The films were heated by simply turning off the cryocooler and allowing the films to warm up.

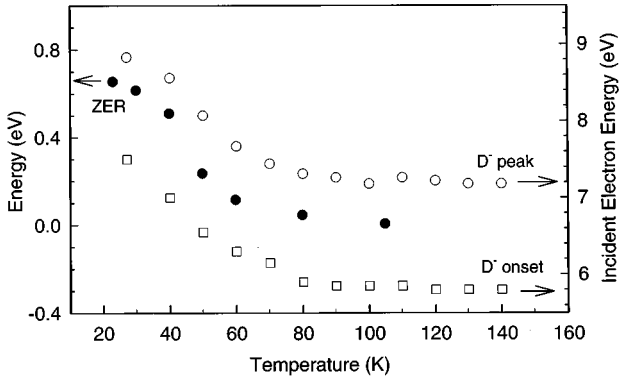

FIG. 5. The ZER of the low-energy electron transmission spectra in Fig. 4 plotted along with the onset and peak energies of the dissociative electron attachment data shown in Fig. 3.

quantitative match (note the different scales on the ordinate axes), there is good qualitative agreement between them. The similarity in their temperature dependence suggests that the changes in the work function and the shift in the DEA resonance energies have a common origin. Although the nature of the transformation that occurs in ice below 60 K is unclear, there is some evidence indicating that vapor-deposited amorphous ice undergoes a gradual structural transition when heated from 38 to 68 K,[60] which may be responsible for the changes observed in the LEET and DEA data in that temperature range.

Figure 6 shows how the energy dependence of the D^- signal changes with temperature for 60 bilayers of porous amorphous and crystalline D_2O ice. The films used to generate Fig. 6 were grown at 90 K (porous amorphous) or 155 K (crystalline), then heated or cooled to the temperature given in the figure for data collection. At sufficiently low temperatures the overall D^- signal is reduced and the $^2B_1$, $^2A_1$, and $^2B_2$ intensities are roughly comparable. The DEA resonances shift to lower energy as the temperature of the film is increased, however, and the ESD yield rises significantly. This effect is greatest for the $^2B_1$ resonance. In addition, the temperatures at which these changes occur and the magnitude of the changes are sensitive to the morphology of the film, as can be seen from a comparison of Figs. 6(a) and 6(b).

It is reasonable to expect the energies and cross sections for exciting DEA resonances in ice to change with the temperature and morphology of the film. The $3s{:}4a_1$ orbital, which is doubly occupied in the three low-energy DEA resonances, is clearly affected by condensation. Rosenberg *et al.* showed that the K-shell excitations of isolated water molecules are severely perturbed and broadened in bulk ice due to interactions between hydrogen atoms on nearby water molecules, and that excitations to the $3s{:}4a_1$ Rydberg orbital apparently only survive in the surface molecules, due to their reduced coordination.[61] It is the diffuse nature of the $3s{:}4a_1$ orbital, which results in significant overlap with neighboring molecules, that leads to its perturbation. Calculations by Goddard and Hunt of the $\langle r^2 \rangle$ expectation value for the electron density of the singlet parent states (5.94 $Å^2$

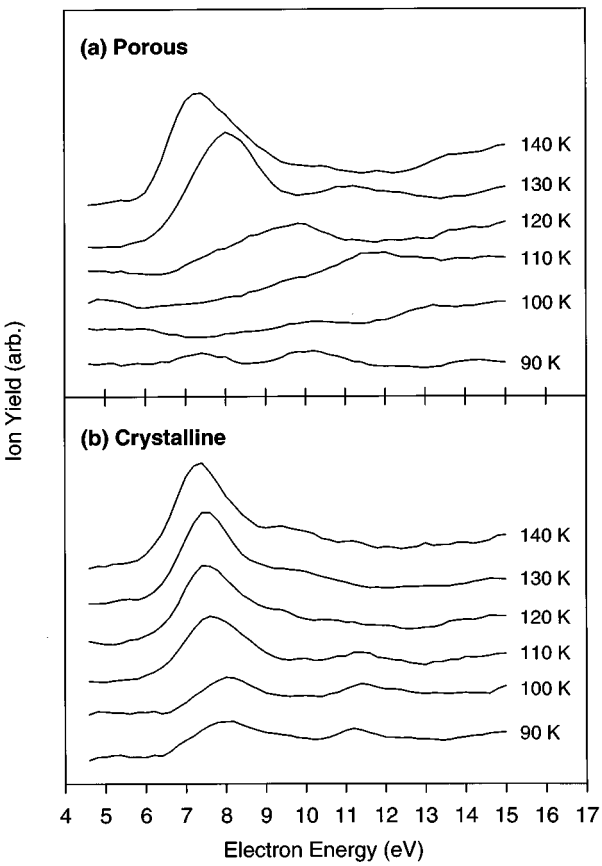

FIG. 6. (a) D^- signal vs incident electron energy, collected at various temperatures from 60-bilayer porous amorphous ice films (grown at 90 K). (b) D^- signal vs incident electron energy, collected at various temperatures from 60-bilayer crystalline ice films (grown at 155 K). Individual scans are offset vertically for display and labeled with the temperature at which they were collected. The films were heated radiantly.

for $^1B_1$ and 7.03 Å^2 for $^1A_1$) indicate that the gas-phase radius of the $3s{:}4a_1$ orbital is comparable to the nearest-neighbor separation in ice (2.8 Å).[47] Rowntree *et al.* suggested that a reduction in the $3s$ Rydberg contribution to the $4a_1$ antibonding orbital, arising from this nearest-neighbor overlap, can explain the shifting and broadening of DEA resonances seen in condensed water.[9] Their assertion is supported by calculations of Winter *et al.*, which show that the inclusion of $3s$ Rydberg orbitals in the CI basis set reduces the calculated energy of the gas-phase $^1B_1$ and $^1A_1$ states by 1.33 and 4.96 eV, respectively.[62] Thus, condensation-induced perturbations of the $3s{:}4a_1$ orbital are probably responsible for the difference between the DEA resonance energies of water vapor and ice, and we suggest that they also contribute to the energy shifts observed as the temperature and morphology of the condensed films are varied.

The energy shifts may also result, in part, from condensation-induced changes in the $1b_1$, $3a_1$, and $1b_2$ bands, since these levels are involved in the three low-energy resonances. Valence-band photoemission studies of thin ice films show that the binding energies and widths of the three highest occupied molecular orbitals of water are affected by condensation and, to a certain degree, by the temperature, thickness and morphology of the film.[31,51,63] If the widths and energies of the levels involved in the DEA resonances change, the DEA resonance energies and lifetimes, and hence the ESD yield, will also change.

Since ice is an insulator, electrostatic charging of the films is a concern as charging could change the apparent energy of the resonances, as well as their ESD yields. However, the experiments presented in this article were performed under essentially charge-free conditions. Under such conditions, experiments carried out in the two labs using incident current densities that vary by nearly two orders of magnitude yield similar results. Also, since the buildup of charge in the film acts differently on oppositely charged ions, the similarity between the temperature dependence of the D^+ and D^- ESD yields from D_2O ice (shown in the following section) reflects, among other things, the film charge neutrality. More details regarding charge trapping in ice films will be presented in a forthcoming publication.[64]

C. Similarity in the D^+ and D^- ESD yields

The temperature dependence of D^+ and D^- ESD yield from ice show some interesting parallels. The D^+ velocity distributions, which are at least bimodal, can be separated into ''fast'' and ''slow'' components.[65] The thickness, morphology, and temperature dependence of the ''slow'' D^+ yield, which arises from $(3a_1)^{-1}(1b_1)^{-1}(4a_1)^{+1}$ or $(3a_1)^{-2}(4a_1)^{+1}$ excitations, are nearly identical to those observed for $(^2B_1)$ D^- ESD.[65] Their similarity is illustrated in Fig. 7, which shows the temperature dependence of the D^- and ''slow'' D^+ ESD yields, each collected from 40-bilayer amorphous and crystalline ice films. Also shown in the figure are D_2O TPD spectra, for comparison. Note that the crystallization temperature for the amorphous film can be determined from the TPD data by observing the point at which the D_2O thermal desorption rate dips (at $\sim$155 K), which is caused by a reduction of the vapor pressure of D_2O upon crystallization.[29,32,33] Although the cations and anions originate from different electronic excitations ($2h1e$ for D^+ and $1h2e$ for D^-), their yields have a nearly identical temperature dependence. This resemblance suggests that the changes in the cation and anion yields with film thickness, temperature, and morphology have a common origin.

Sieger, Simpson, and Orlando attribute the rise in the D^+ ESD yield with temperature to a thermally activated reduction in surface hydrogen bonding which increases the lifetimes of the excited states responsible for ion desorption, especially those excited states that involve the a_1 bands of ice.[65] Since the excitations that lead to D^- and low-energy D^+ desorption both involve occupation of the $4a_1$ level, which is strongly influenced by nearest-neighbor interactions, it is likely that thermally induced changes in the lifetime and energy of the $4a_1$ level are primarily responsible for the temperature dependence of the D^+ and D^- ESD yields. Moreover, since the increase in the ESD yield with temperature occurs at the point where the generation and transfer of defects becomes feasible,[44,66,67] we suggest that the enhanced lifetimes at elevated temperatures result from a

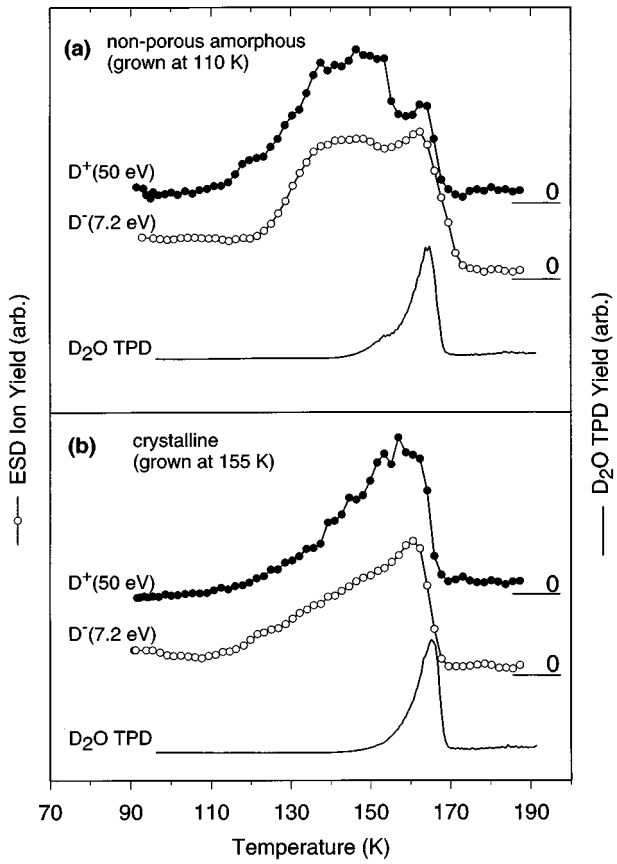

FIG. 7. (a) D^- signal vs temperature (90→190 K, at 8 K/min) collected with $E_i = 7.2$ eV from a 40-bilayer nonporous amorphous ice film. (b) D^- signal vs temperature (90→190 K, at 8 K/min) collected with $E_i = 7.2$ eV from a 40-bilayer crystalline ice film. Plotted along with the D^- signal is the low-energy D^+ signal collected from identical films with $E_i = 50$ eV (see Ref. 65). Also shown are the corresponding D_2O thermal desorption spectra, for comparison. The zeroes for the D^- and D^+ data are indicated in the figure.

weakening of the hydrogen bonding network, which reduces the effective overlap between adjacent molecules, thereby increasing the lifetime of an excitation localized on a particular molecule.

D. Reversible and irreversible phase transitions

A number of structural changes occur in ice as the temperature is raised. The density of ice generally decreases with increasing temperature,[68] with one apparent exception. As porous amorphous ice is heated to ~120 K it undergoes a structural transition in which the pores collapse and the density actually *increases* from 0.6 to 0.9 g/cm^3.[39–43] Ice also goes through a reversible ''glass transition,'' whose temperature (T_g) has been reported to be anywhere from 124 to 137 K for amorphous ice[44,66] and ~140 K for cubic crystalline ice.[67] Below T_g, inherent disorder in the proton sublattice is frozen in whereas, above T_g, enhanced proton mobility enables configurational rearrangement of the hydrogen network through molecular reorientation, accompanied by the formation and transfer of Bjerrum defects. The energy needed to form Bjerrum defects is ~300 meV,[69] while the energy required to mobilize *pre-existing* defects is somewhat lower.[70] In a typical ice film there are a large number of pre-existing Bjerrum L defects (i.e., missing hydrogen bonds), which form as the film is grown.[69] In fact, the volume density of these defects can be as high as ~10^{19} cm^{-3} near the surface,[71] yielding an area density of 10^{12}–10^{13} cm^{-2} (roughly one defect for every 10^2–10^3 surface molecules). These L defects, whose formation and transport is expected to weaken the hydrogen bonding network, become mobile at temperatures as low as ~100 K for amorphous ice and ~130 K for crystalline ice.[72,73] At sufficiently high temperatures, amorphous ice crystallizes. Crystallization has been reported to occur at temperatures ranging from 145 to 172 K,[33,42,44,72] depending on the heating rate used. The crystallization of amorphous ice is, in fact, a kinetically limited process whose activation energy has been determined to be 67 kJ/mol.[32]

The intensity of the D^- ESD signal arising from the excitation of the $^2B_1$ DEA resonance at ~7 eV changes dramatically with temperature, and its temperature dependence varies with the morphology of the film. The thermally induced changes in the ($^2B_1$) ESD yield seem to correspond with known phase transitions in ice. A comparison of the ($^2B_1$) D^- temperature dependence for 60-bilayer films of porous (open circles) and nonporous amorphous ice (filled circles) is shown in Fig. 8(a). Between 110 and 130 K the D^- signal from the porous film is greater than that from the nonporous film. This result is highly reproducible. Since the micropores are the only significant difference between the two ice polymorphs, the dissimilarity in their ESD yield in this temperature range likely results from the presence of the pores. Figure 8(b) shows what happens to the ($^2B_1$) D^- signal from a 60-bilayer film of porous ice if its temperature is ramped to 130 K (open circles) and then brought back down to 90 K before heating it up to 190 K (filled circles). Annealing the film to ~130 K, which is expected to collapse the pores, causes an irreversible change in the temperature dependence of the D^- yield so that it mimics the behavior seen in the nonporous film grown at 110 K. This indicates that the ESD yield is sensitive to the presence of the pores and, in fact, may be useful in monitoring pore collapse.

Figure 9(a) shows a comparison of the ($^2B_1$) D^- temperature dependence for 60-bilayer films of nonporous amorphous (open circles) and crystalline ice (filled circles). There is a clear difference in their ion yields between ~125 and 160 K. The D^- signal from the amorphous film rises significantly above that from the crystalline film at ~125 K, then drops back down at 155–160 K. The D^- yield from the crystalline film increases with temperature, with an onset at ~135 K. This increase is reversible, in the sense that heating the ice causes the signal to rise monotonically whereas cooling it down causes the signal to drop. This can be repeated several times with essentially the same results if the temperature is kept below the onset for appreciable thermal desorption. The increase in D^- signal from the amorphous film also appears to be reversible as long as the film remains amorphous. These reversible increases in the ion yield, at ~125 K for amorphous ice and at ~135 K for crystalline ice, do not

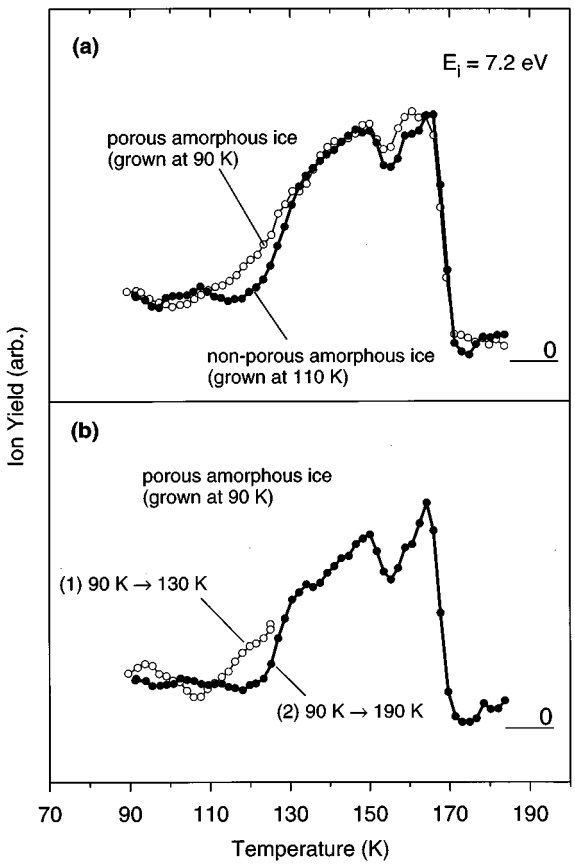

FIG. 8. (a) D^- signal vs temperature (90→190 K, at 8 K/min), collected with $E_i = 7.2$ eV from 60-bilayer porous and nonporous amorphous ice films. (b) D^- signal vs temperature (90→130→90→190 K), collected from a 60-bilayer porous amorphous ice film, using the same incident electron energy. For clarity, the first part of the temperature ramp (90→130 K) is shown as open circles and the final part (90→190 K) is shown as filled circles. The zeroes for the D^- data are indicated in the figure.

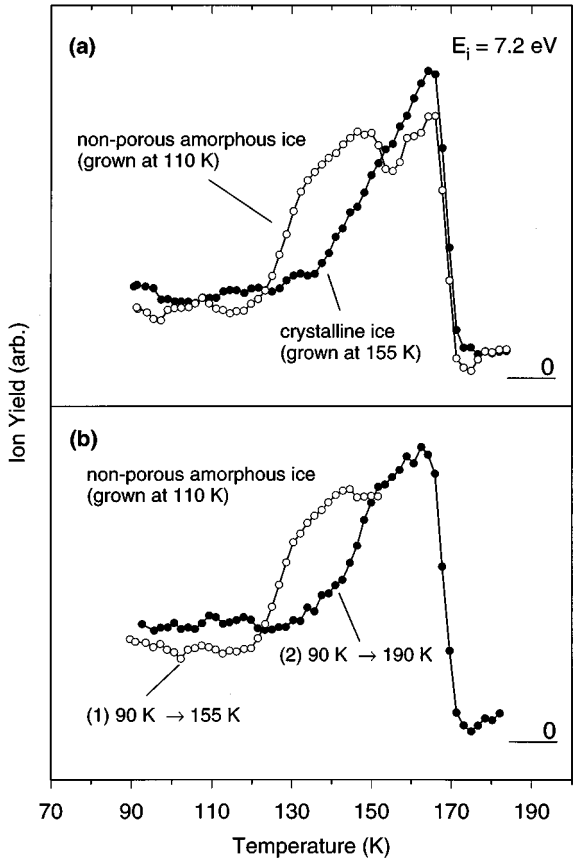

FIG. 9. (a) D^- signal vs temperature (90→190 K, at 8 K/min), collected with $E_i = 7.2$ eV from 60-bilayer nonporous amorphous and crystalline ice films. (b) D^- signal vs temperature (90→155→90→190 K), collected from a 60-bilayer nonporous amorphous ice film, using the same incident electron energy. For clarity, the first part of the temperature ramp (90→155 K) is shown as open circles and the final part (90→190 K) is shown as filled circles. The zeroes for the D^- data are indicated in the figure.

correlate with any known structural transitions in ice, but they are consistent with the aforementioned glass transitions in ice. Since the glass transitions are reversible and occur at roughly the same temperatures at which the D^- yield increases, it is likely that the rise in the D^- signal with temperature is related to the changes that occur in ice when the proton sublattice becomes mobile.

Figure 9(b) shows how the $(^2B_1)$ D^- signal changes if a porous amorphous film is heated to 155 K (open circles) and then cooled back down to 90 K before ramping the temperature to 190 K (filled circles). This preannealing cycle is expected to crystallize the amorphous film. An irreversible change in the temperature dependence of the yield is observed, as a result of the annealing, and the D^- temperature dependence from the annealed film resembles that from a crystalline film grown at 155 K. Hence, the ESD yield is also sensitive to the crystallinity of the film, and could possibly be used to monitor crystallization.

E. Thermally induced changes in surface structure

The ESD yield derives almost entirely from the molecules comprising the outermost few layers of the surface. Hence, any changes in the surface structure brought about by a decrease in the degree of hydrogen bonding near the surface should have a strong effect on the ESD yield. A recent set of studies have shown that at sufficiently low temperatures the surface of ice has a large number of molecules in 3- and 4-coordinate geometries, with fewer dangling O–H bonds than an ideally terminated surface.[74–76] The increased coordination is apparently due to surface molecules that twist away from their ideal bulk-terminated positions to form additional hydrogen bonds with molecules in the bulk. Although this increases the strain at the surface, it reduces the overall surface free energy. One might expect that a weakening of the hydrogen bonding network near the surface would enable this highly strained surface to relax toward a bulklike termination having more 2- and 3-coordinate molecules. In a study of H^+ desorption from H_2O, Rosenberg *et al.* noted that there are basically six types of surface sites on ice and suggested that the configurations having one or both O–H bonds pointing away from the surface generally have higher ESD cross sections than those whose O–H bonds point toward other water molecules in the film.[77] This implies that a surface terminated with many 3- and 4-

coordinate molecules has a relatively low ESD cross section. However, if heating causes it to relax to a more bulklike termination, the ESD yield should increase since the surface molecules will be in configurations with one or more O–H bonds pointing toward the vacuum. Although this is surely occurring to some extent, its contribution to the overall increase in the ion yield with temperature is unclear.

IV. CONCLUSIONS

In summary, we observe four features in the ESD of D^- from condensed D_2O films. The three lowest energy features are identified with the formation of $^2B_1$, $^2A_1$, and $^2B_2$ DEA resonances. The fourth is likely due to another resonance that either decays via dissociative attachment and/or decays into an excited state that dissociates into an ion pair. The DEA resonance energies and their ion desorption yields change with film temperature and morphology. Some of the energy shift is due to work function variations that occur in films grown at extremely low temperatures. The remaining shift is due to changes in the electronic structure of the water molecules brought about by interactions with their nearest neighbors. The ($^2B_1$) D^- yield is found to increase with temperature, but it deviates from this trend at temperatures corresponding to structural phase transitions in bulk ice. Similar behavior is observed in the ESD of low-energy D^+ ions from D_2O ice. The general increase in D^+ and D^- yields with temperature is consistent with thermally induced changes in the hydrogen bonding network brought about by defect formation and transport, which affect the lifetimes of the predissociative states that lead to ESD, especially those involving the a_1 levels. The deviations in the D^- signal at temperatures corresponding to irreversible structural phase transitions in bulk ice also suggest that the ice structure, particularly at the surface, influences the ion yield. While raising the temperature affects both the structure of the surface and the strength of the hydrogen bonding network, further investigation is required to determine the relative contribution of each to the changes observed in the ESD yield.

ACKNOWLEDGMENTS

The authors thank R. S. Smith, G. A. Kimmel, and B. D. Kay for useful discussions. We also thank G. A. Kimmel for technical assistance during the initial stages of the experiments. The work at PNNL was supported by the U.S. Department of Energy Office of Basic Energy Sciences, Chemical Physics Program, and by Associated Western Universities Inc. under Grant DE-FG07-93ER-75912 or DE-FG07-94ID-13228 with the U.S. Department of Energy. PNNL is operated for the Department of Energy by Battelle Memorial Institute under Contract No. DE-AC06-76RLO 1830. The work at the University of Sherbrooke was supported by the Medical Research Council of Canada. W.C.S. and M.T.S. are Associated Western Universities Postdoctoral Fellows.

[1] R. E. Palmer, Prog. Surf. Sci. **41**, 51 (1992).
[2] R. E. Palmer and P. J. Rous, Rev. Mod. Phys. **64**, 383 (1992).
[3] L. Sanche, *Excess Electrons in Dielectric Media*, edited by C. Ferrandi and J. P. Jay-Gerin (CRC, Boca Raton, 1991), Chap. 1.
[4] L. Sanche, Scanning Microscopy **9**, 619 (1995).
[5] L. Sanche, J. Phys. B: At. Mol. Opt. Phys. **23**, 1597 (1990).
[6] R. Azria, L. Parenteau, and L. Sanche, Chem. Phys. Lett. **171**, 229 (1990).
[7] M. A. Huels, L. Parenteau, and L. Sanche, J. Chem. Phys. **100**, 3940 (1994).
[8] M. Michaud and L. Sanche, Phys. Rev. Lett. **59**, 645 (1987).
[9] P. Rowntree, L. Parenteau, and L. Sanche, J. Chem. Phys. **94**, 8570 (1991).
[10] P. Rowntree, L. Sanche, L. Parenteau, M. Meinke, F. Welk, and E. Illenberger, J. Chem. Phys. **101**, 4248 (1994).
[11] L. Sanche, A. D. Bass, P. Ayotte, and I. I. Fabrikant, Phys. Rev. Lett. **75**, 3568 (1995).
[12] M. Tronc, R. Azria, Y. Le Coat, and E. Illenberger, J. Phys. Chem. **100**, 14 745 (1996).
[13] R. C. Weast, *Handbook of Chemistry and Physics*, 53rd ed. (CRC, Cleveland, 1972).
[14] D. S. Belic, M. Landau, and R. I. Hall, J. Phys. B: At. Mol. Opt. Phys. **14**, 175 (1981).
[15] R. N. Compton and L. G. Christophorou, Phys. Rev. **154**, 110 (1967).
[16] M. G. Curtis and I. C. Walker, J. Chem. Soc. Faraday Trans. **88**, 2805 (1992).
[17] B. C. DeSouza and J. H. Green, Nature **203**, 1165 (1964).
[18] F. H. Dorman, J. Chem. Phys. **44**, 3856 (1966).
[19] M. A. D. Fluendy and I. C. Walker, J. Chem. Soc. Faraday Trans. **91**, 2249 (1995).
[20] M. Jungen, J. Vogt, and V. Staemmler, Chem. Phys. **37**, 49 (1979).
[21] M. M. Mann, A. A. Hustrulid, and I. T. Tate, Phys. Rev. **58**, 340 (1940).
[22] C. E. Melton and G. A. Neece, J. Chem. Phys. **55**, 4665 (1971).
[23] C. E. Melton, J. Chem. Phys. **57**, 4218 (1972).
[24] E. E. Muschlitz, Jr. and T. L. Bailey, J. Phys. Chem. **60**, 681 (1956).
[25] E. E. Muschlitz, Jr., J. Appl. Phys. **28**, 1414 (1957).
[26] G. J. Schulz, J. Chem. Phys. **33**, 1661 (1960).
[27] G. Seng and F. Linder, J. Phys. B: At. Mol. Opt. Phys. **9**, 2539 (1976).
[28] P. Rowntree, L. Parenteau, and L. Sanche, Chem. Phys. Lett. **182**, 479 (1991).
[29] M. Akbulut, N. J. Sack, and T. E. Madey, Surf. Sci. **351**, 209 (1996).
[30] G. B. Fisher and J. L. Gland, Surf. Sci. **94**, 446 (1980).
[31] G. B. Fisher, General Motors Research Publications GMR-4007 PCP-171, 1982.
[32] R. S. Smith, C. Huang, E. K. L. Wong, and B. D. Kay, Surf. Sci. **367**, L13 (1996).
[33] R. J. Speedy, P. G. Debenedetti, R. S. Smith, C. Huang, and B. D. Kay, J. Chem. Phys. **105**, 240 (1996).
[34] Note that many studies report film thicknesses in terms of monolayers of ice. This leads to some ambiguity since some use half a bilayer (0.5×10^{15} molecules/cm^2) to define a monolayer, while others use twice this value. To avoid this ambiguity, we report thicknesses in bilayers.
[35] More noticeable effects were apparent in the kinetic energy distributions of D^+ ions collected under identical conditions. See Ref. 65.
[36] L. Sanche, J. Chem. Phys. **71**, 4860 (1979).
[37] R. M. Marsolais and L. Sanche, Phys. Rev. B **38**, 11 118 (1988).
[38] P. Cloutier and L. Sanche, Rev. Sci. Instrum. **60**, 1054 (1989).
[39] B. S. Berland, D. E. Brown, M. A. Tolbert, and S. M. George, Geophys. Res. Lett. **22**, 3493 (1995).
[40] D. E. Brown, S. M. George, C. Huang, E. K. L. Wong, K. B. Rider, R. S. Smith, and B. D. Kay, J. Phys. Chem. **100**, 4988 (1996).
[41] J. A. Ghormley, J. Chem. Phys. **48**, 503 (1968).
[42] G. P. Johari, A. Hallbrucker, and E. Mayer, J. Chem. Phys. **95**, 2955 (1991).
[43] B. Rowland and J. P. Devlin, J. Chem. Phys. **94**, 812 (1991).
[44] G. P. Johari, A. Hallbrucker, and E. Mayer, J. Chem. Phys. **92**, 6742 (1990).
[45] I. N. Levine, *Quantum Chemistry*, 4th ed. (Prentice Hall, Englewood Cliffs, NJ, 1991).
[46] P. A. Thiel and T. E. Madey, Surf. Sci. Rep. **7**, 211 (1987).
[47] W. A. Goddard III and W. J. Hunt, Chem. Phys. Lett. **24**, 464 (1974).
[48] B. Baron and F. Williams, J. Chem. Phys. **64**, 3896 (1976).
[49] B. Baron, D. Hoover, and F. Williams, J. Chem. Phys. **68**, 1997 (1978).
[50] M. J. Campbell, J. Liesegang, J. D. Riley, R. C. G. Leckey, J. G. Jenkin, and R. T. Poole, J. Electron. Spectrosc. Rel. Phenom. **15**, 83 (1979).

[51] E. Langenbach, A. Spitzer, and H. Lüth, Surf. Sci. **147**, 179 (1984).
[52] D. E. Ramaker, Chem. Phys. **80**, 183 (1983).
[53] M. U. Sander, K. Luther, and J. Troe, Ber. Bunsenges. Res. **97**, 953 (1993).
[54] T. Shibaguchi, H. Onuki, and R. Onaka, J. Phys. Chem. Soc. Jpn. **42**, 152 (1977).
[55] V. F. Petrenko and I. A. Ryzhkin, Phys. Rev. Lett. **71**, 2626 (1993).
[56] G. P. Parravicini and L. Resca, Phys. Rev. B **8**, 3009 (1973).
[57] P. Rowntree, H. Sambe, L. Parenteau, and L. Sanche, Phys. Rev. B **47**, 4537 (1993).
[58] W. C. Simpson, L. Parenteau, R. S. Smith, L. Sanche, and T. M. Orlando, Surf. Sci. (in press).
[59] G. A. Kimmel and T. M. Orlando, Phys. Rev. Lett. **77**, 3983 (1996).
[60] P. Jenniskens and D. F. Blake, Science **265**, 753 (1994).
[61] R. A. Rosenberg, P. R. LaRoe, V. Rehn, J. Stöhr, R. Jaeger, and C. C. Parks, Phys. Rev. B **28**, 3026 (1983).
[62] N. W. Winter, W. A. Goddard III, and F. W. Bobrowicz, J. Chem. Phys. **62**, 4325 (1975).
[63] D. Schmeisser, F. J. Himpsel, G. Hollinger, B. Reihl, and K. Jacobi, Phys. Rev. B **27**, 3279 (1983).
[64] W. C. Simpson, T. M. Orlando, L. Parenteau, K. Nagesha, and L. Sanche (in preparation).
[65] M. T. Sieger, W. C. Simpson, and T. M. Orlando, Phys. Rev. B **56**, 4925 (1997).
[66] J. P. Handa and D. D. Klug, J. Chem. Phys. **92**, 3323 (1988).
[67] O. Yamamuro, M. Oguni, T. Matsuo, and H. Suga, J. Phys. Chem. Solids **48**, 935 (1987).
[68] V. F. Petrenko, U.S. Army Corps of Engineers Special Report **93–25**, 1993.
[69] V. F. Petrenko and R. W. Whitworth, U.S. Army Corps of Engineers Special Report **94–4**, 1994.
[70] I. Takei and N. Maeno, J. Phys. Colloq. (France) **48**, 121 (1987).
[71] H. Dosch, A. Lied, and J. H. Bilgram, Surf. Sci. **327**, 145 (1995).
[72] M. Fisher and J. P. Devlin, J. Phys. Chem. **99**, 11 584 (1995).
[73] P. J. Wooldridge and J. P. Devlin, J. Chem. Phys. **88**, 3086 (1988).
[74] L. Delzeit, M. S. Devlin, B. Rowland, J. P. Devlin, and V. Buch, J. Phys. Chem. **100**, 10 076 (1996).
[75] J. P. Devlin and V. Buch, J. Phys. Chem. **99**, 16 534 (1995).
[76] B. Rowland, N. S. Kadagathur, J. P. Devlin, V. Buch, T. Feldman, and M. J. Wojcik, J. Chem. Phys. **102**, 8328 (1995).
[77] R. A. Rosenberg, V. Rehn, V. O. Jones, A. K. Green, C. C. Parks, G. Loubriel, and R. H. Stulen, Chem. Phys. Lett. **80**, 488 (1981).